# Elucidating the structure of the graphitic carbon nitride nanomaterials using X-ray photoelectron spectroscopy and X-ray powder diffraction techniques

Emilia Alwin, Waldemar Nowicki, Robert Wojcieszak, Michal Zieliński, Mariusz Pietrowski

## ARTICLE

# Elucidating the structure of the graphitic carbon nitride nanomaterials using X-ray photoelectron spectroscopy and X-ray powder diffraction techniques

Emilia Alwin[a,b], Waldemar Nowicki[a], Robert Wojcieszak[b], Michał Zieliński[a] and Mariusz Pietrowski[a*]

By using the most popular method of the graphitic carbon nitride synthesis (gCN) – the thermal condensation of dicyandiamide in a semi-closed system, carbon nitrides were obtained at 500, 550, and 600 °C. The resulting materials were comprehensively analyzed by X-ray photoelectron spectroscopy (XPS) and X-ray powder diffraction (XRD) methods. We showed that the use of routine analytical methods permit to give insight into the structure of the carbon nitride materials. The results obtained indicate that the prepared carbon nitrides have a layered structure irrespective of the synthesis temperature. However, individual layers are not fully-condensed poliheptazine network but they consist of the chains of poly(aminoimino)heptazine (known as Liebig's melon). With a rise in the condensation temperature, the degree of condensation and the degree of structural order increases, the interplanar spacing $d$ decreases and the number of condensed layers increases. The analysis of geometric linear structures and a fully condensed structure for polymeric carbon nitride was performed and the ranges within which the contents of different nitrogen species (pyridine, amine, imine and quaternary nitrogen) can change were determined. These data in conjunction with the results of quantitative XPS analysis permit a correct identification of the carbon nitride structure. Our results showed that XPS studies should include both qualitative and quantitative analyses to enable correct identification of the carbon nitride structure. The XRD method proved that the 3D crystal structure of carbon nitride is described more correctly by the orthorhombic cell and space group P2₁2₁2 applied to condensed chains of poly(aminoimino)heptazine (melon) and not by hexagonal cell with the space group P6m2.

## 1. Introduction

A meteoric career of graphitic carbon nitride (gCN–C₃N₄) as a solar-driven, metal-free photocatalyst began in 2009 with the paper of Wang and Antonietti.[1] In the age of increasing environmental awareness, it hit on the fertile ground opening a new window of opportunities for the development of a cheap method for hydrogen production using visible light.[2-4] As time went by, it became evident that the photocatalytic activity of gCN is insufficient, mainly because of the fast recombination of electron-hole pairs. Several attempts have been made to improve gCN properties by its doping with heteroatoms,[5-9] synthesis of nanostructural carbon nitrides with unique morphology and large surface area,[10-14] the formation of nanocomposites,[15-17] and subjecting to exfoliation.[18-22] Many of these attempts resulted in improved activity, however, these methods are labor-intensive and expensive which causes their

application on a commercial scale is doomed to failure. Still, the simplest and the cheapest method of graphitic carbon nitride synthesis is the thermal condensation of cheap and easily available materials such as urea, thiourea, cyanamide, dicyandiamide, and melamine.[23-29] Carbon nitride obtained by the above-mentioned method was characterized many times but despite this, controversies concerning its structure and composition still exist. This was pointed out by Miller et al.[30, 31] and Kessler et al.,[32] who expressed the opinion that it is unjustified to use the term "graphitic carbon nitride" for a wide range of materials of diverse compositions. A vast majority of materials described by the formula C₃N₄ are, in fact, microcrystalline materials containing hydrogen in their structure and should be described by the formula $C_xN_yH_z$ or called Liebig's melon with the formula C₂N₃H. The aforementioned authors have proposed to label these materials as gCN and we followed this proposition in our work. Also the structure of gCN arouses many controversies. Models based on s-triazine and tri-s-triazine (heptazine) were proposed.[33-35] Theoretical considerations showed that the tri-s-triazine-based model is energetically favored compared to that based on s-triazine subunit as it was confirmed by DFT studies.[33-35] Heptazine subunits can combine *via* tertiary nitrogen into fully condensed structure (Fig. 1a) which forms layers set one above the other just as in a graphite material (Fig. 1c). Another

a. Faculty of Chemistry, Adam Mickiewicz University in Poznań, Uniwersytetu Poznańskiego 8, 61-614 Poznań, Poland.
b. Univ. Lille, CNRS, Centrale Lille, Univ. Artois, UMR 8181 - UCCS - Unité de Catalyse et Chimie du Solide, F-59000 Lille, France.
c. *E-mail: mariop@amu.edu.pl

possibility consists in combining the heptazine subunits into melon chains (Fig. 1b) which also form layers through hydrogen interactions (Fig. 1d). The discrimination between both types of structures is difficult. Thus development of new methods for the exact structure determination is of high importance.

Herein we conducted detailed XPS and XRD studies of the graphitic carbon nitride derived by thermal condensation of dicyandiamide to prove that these methods can be easily employed to describe and confirm the exact structure of the graphitic carbon nitride. We showed that the method of thermal condensation, used in this work, enable to obtain, irrespective of temperature, carbon nitride built of melon chains and not fully-condensed graphitic carbon nitride.
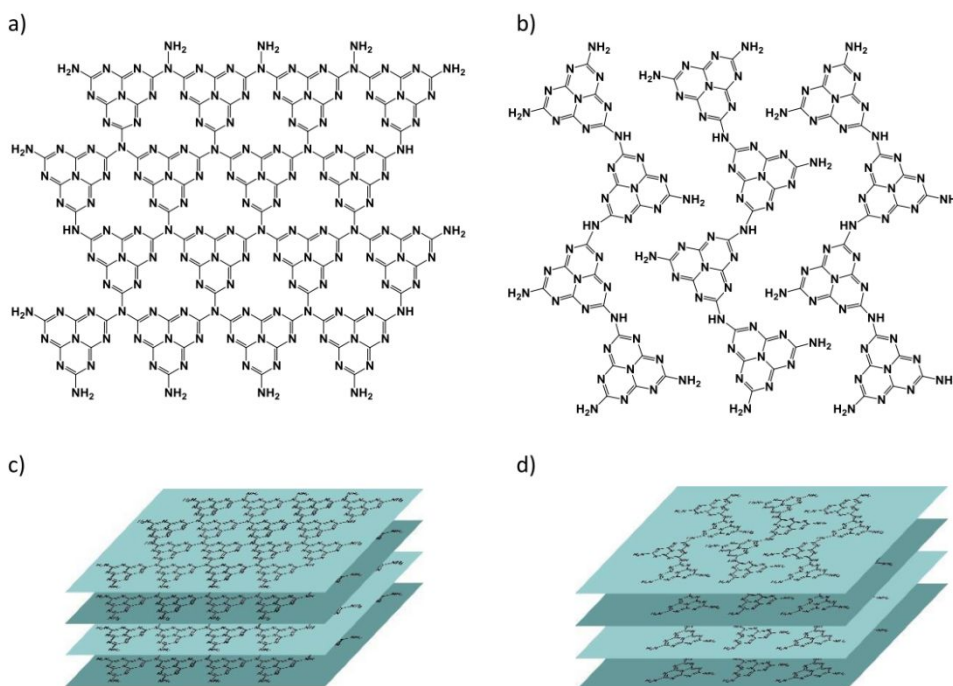


Fig. 1 The structure of graphitic carbon nitride. a) and c) represent fully condensed structure; and b) and d) melon-type structure (according to Ref. [36]).

## 2. Experimental Section

### 2.1. Preparation of graphitic carbon nitride

Graphitic carbon nitride was prepared by the pyrolysis of dicyandiamide (DCDA) (Sigma-Aldrich, 99%) in a semi-closed system according to a defined procedure. Typically, 4 g of DCDA precursor was put into a quartz crucible (~50 mL) with a cover and heated at 500, 550, or 600 °C in a muffle furnace for 4h with a heating rate of 10 °C·min$^{-1}$ under ambient pressure in the air. The crucible was allowed to remain in the furnace until it cooled down to room temperature. The obtained yellow material was ground into a fine powder in an agate mortar. The powder was stored in a desiccator over molecular sieves 4A. The samples were labeled with codes D-500, D-550, and D-600, where the number designates synthesis temperature in °C.

### 2.2. X-ray photoelectron spectroscopy (XPS)

The XPS study was aimed at analyzing chemical bonding and elemental composition. A Kratos Axis Ultra spectrometer (Kratos Analytical, UK) was used. The base pressure during spectra acquisition was better than 10$^{-6}$ Pa and was achieved using an ion pump with cryoshroud (220 L·s$^{-1}$). The excitation source was monochromatized aluminum K$\alpha$ radiation (1486.6 eV) operated at 10 mA and 15 kV. The recorded spectra included wide and narrow scans and the total acquisition time was approximately 1 hour. The spectra were acquired sequentially. The calibration and linearity of the binding energy scale were confirmed and charge stabilization was achieved by using the Kratos Axis device. With the selected scan parameters, the full width at half maximum (FWHM) of the Ag 3d$_{5/2}$ peak of a standard silver sample was about 0.9 eV. The size of the analyzed sample area was about 700 μm x 300 μm. The sample powders were pressed into small stainless steel troughs mounted on a multi-specimen holder, before loading into the spectrometer. The transfer procedure within the spectrometer included exposure to the pumping system for 10 hours before conducting the XPS analyses. The pass energy of the hemispherical analyzer was set at 160 eV for the wide scan and 40 eV for narrow scans. The charge referencing method used was the C–(C, H) component of the C 1s peak of adventitious carbon fixed at 284.6 eV. The data treatment was performed using CasaXPS software (Casa Software Ltd., UK). Molar fractions were calculated using peak areas normalized on the

basis of acquisition parameters after a Shirley background subtraction and corrected with experimental sensitivity factors and transmission factors provided by the manufacturer. The description of the XPS procedure was based on the guidelines from the paper by Greczynski and Hultman.[37]

### 2.3. X-ray powder diffraction (XRD)

The powder X-ray diffraction patterns of the samples were obtained using a Bruker D8 Advance diffractometer with Ge-monochromatized CuK$\alpha$ radiation (λ = 1.5406 Å). The XRD data were collected over a 2-theta range of 5 − 80° with a step size of 0.01° and the scanning time rate of 5 seconds. The parameters describing the diffractograms and the unit cell parameter values were determined using Winplotr and UnitCell programs, respectively.[38, 39] The structure models used for the refinement of gCN were placed in the Electronic Supplementary Material (ESI).

## 3. Results and discussion

### 3.1. Structure analysis by X-ray photoelectron spectroscopy (XPS)

The XPS study can provide valuable information on the structure of carbon nitride (both qualitative and quantitative one) and about the content of respective elements and their forms. The interpretation is, however, difficult because of the ambiguity of assignment of respective signals to specific species, particularly concerning the N 1s of nitrogen.[40] In the case of C 1s signal, there is quite a high agreement to assign the signal at ∼288.2(4) eV to $sp^2$-bonded carbon (N−C≡N) in the triazine or heptazine rings and the signal at ∼284.6(8) eV to graphitic carbon (**C**−[C,H] adventitious carbon, AdC) which usually serves for energy calibration.[41] On the other hand, the interpretation of nitrogen signals N 1s arouses controversy. Usually, three main signals observed at binding energies (BE) of ∼398.6, 399.7, 401.1 eV are ascribed to pyridinic nitrogen (denoted here as Py), tertiary nitrogen N−(C)$_3$, i.e. the central nitrogen of the heptazine ring (also called quaternary; denoted as Q) and amino −NH$_2$ or −NH− or pyrrolic (denoted as NH$_x$) groups, respectively.[16, 41-45]

There are also other interpretations according to which the signals at 399.7 and 401.1 eV are ascribed to NH$_x$ and quaternary nitrogen (Q), i.e. ascribed reversely. Already in 1987 Bartle, Perry and, Wallace,[46] while studying model compounds, determined the following sequence for different forms of nitrogen, additionally distinguishing amino nitrogen:

Py  -  398.7 eV  pyridine type (for phenanthridine and phenazine),
NH$_2$  -  399.4 eV  primary amines (for 1-aminopyrene, 1-aminofluorene),
NH  -  400.3 eV  pyrrole type (secondary amines) (for 13H-dibenzo[a,i]carbazole and carbazole),
Q  -  401.4 eV  quaternary nitrogen.

Also, the some authors[47] suggested that the shoulder observed at 399.3 eV can origin from the nitrogen in −NH$_2$ group. The above ascription was confirmed many times in later papers (Table 1).

**Table 1** N 1s core level binding energies for graphitic carbon nitride. The respective forms of nitrogen were numbered according to increasing binding energy sequence: N1, N2, N3, N4. In parentheses, the difference in BE was shown between a given band and N 1s band of pyridinic nitrogen (N1).

| No. | Ref. | Py (N1) | −NH$_2$ (N2) | −NH− (N3) | Q (N4) |
|---|---|---|---|---|---|
| 1 | 46 | 398.7 | 399.4(0.7) | 400.3(1.6) | 401.4(2.7) |
| 2 | 48 | 398.3 | 399.1(0.8) | 400.1(1.8) | 401.3(3.0) |
| 3 | 49 | 398.7 | 399.1(0.4) | 400.4(1.7) | 401.4(2.7) |
| 4 | 50 | 398.2 | 399.1(0.9) | 400.3(2.1) | - |
| 5 | 51 | 398.5 | - | 400.5(2.0) | 401.1(2.6) |
| 6 | 52 | 398.8 | 399.4(0.6) | 400.2(1.4) | 401.4(2.6) |
| 7 | 53 | 398.3 | 399.2(0.9) | 400.1(1.8) | 401.4(3.1) |
| 8 | 47 | 398.9 | 399.5(0.6) | 400.6(1.7) | 401.5(2.6) |
| 9 | Average | 398.6 | 399.3(0.70) | 400.3(1.76) | 401.4(2.76) |
| 10 | D-500* | 398.7 | 399.6(0.9) | 400.5(1.8) | 401.4(2.7) |
| 11 | D-550* | 398.7 | 399.5(0.8) | 400.4(1.7) | 401.4(2.7) |
| 12 | D-600* | 398.7 | 399.4(0.8) | 400.3(1.7) | 401.3(2.6) |

* Our results

Absolute values of binding energies of respective signals depend on the value assumed during the spectra calibration, whereas differences in BE (the values are shown in parentheses in Table 1) between a respective band and the pyridinic nitrogen Py(N1) band are characterized by a good agreement. This lends credence to the assumed interpretation and signal ascription.

The study of Akaike et al. [47] (Table 1, entry 8) seems to dissipate the controversy concerning the assignment of bands. The authors proved that the signal appearing at the highest binding energy in the N 1s range (around 401.5 eV) originates from the N−(C)$_3$ component (quaternary nitrogen − Q).[47] Moreover, they have found that the signals originating from primary and secondary amines can be split and that binding energy of primary amines is lower than that of secondary amines. The assignment of bands was summarized in Figure 2. The respective forms of nitrogen were numbered according to the increasing binding energy sequence: N1, N2, N3, N4.

Analysis of data presented in Table 1 and conclusions drawn by Akaike et al.[47] induced us to accept this method for the interpretation of XPS spectra measured in our work.

The survey spectrum of D-600 (Fig. 3a) showed that the sample was composed solely of C, N, and O, which may have originated from adsorbed water molecules.[15, 36, 54, 55]
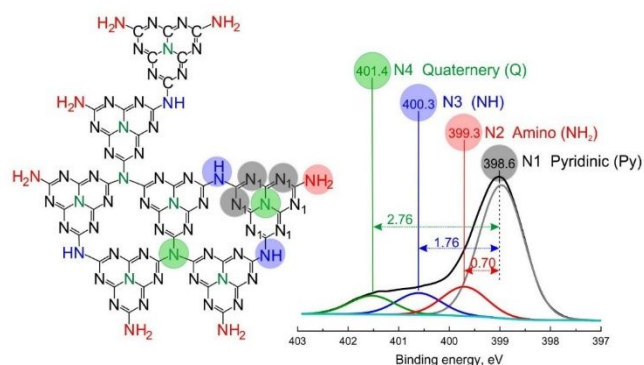


**Fig. 2** The binding energy of N 1s signal in the XPS spectra and assignment to specific nitrogen signals.
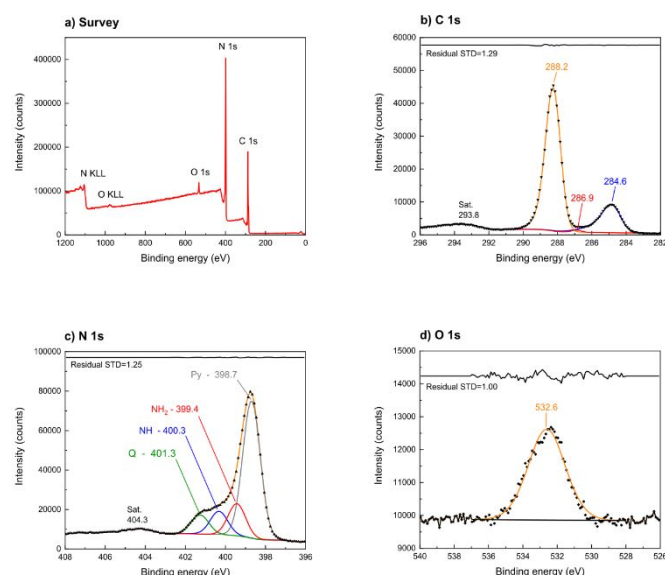
**Fig. 3** XPS survey spectrum of carbon nitride (D-600) (a) and spectra of C 1s (b), N 1s (c), and O 1s (d). Peaks labelled as Sat. at 293.8 and 404.3 eV are attributed to the shake-up satellites. Spectroscopic data were processed by the CasaXPS software using a peak-fitting routine with Shirley background and asymmetrical Voigt functions.

The C 1s XPS spectra of the D-600 sample (Fig. 3b) contained two dominant components located at 284.6 and 288.2 eV, corresponding to graphitic carbon (**C**–[C,H] adventitious carbon, AdC), and N–C=N in the triazine or heptazine rings, respectively. To get a better fitting of the spectra, it was necessary to introduce the third signal with a maximum at 286.9 eV. In the case of the D-600 sample, its contribution to the N 1s signal is ~0.7 %, in that of the D-550 sample it is somewhat less (~0.4 %) and the D-500 sample does not contain it at all (see Table 2). In general, this signal is greater in the case of the samples synthesized at higher temperatures. It can be thus ascribed to nitrile species $-C\equiv N$.[56-60] Another nitrile species signal visible in N 1s region is at ~400.2 eV (it will be discussed later). Dante et al.[61] observed nitrile species formation during the calcination of carbon nitride at high temperatures. They claim that the thermal degradation of the graphitic carbon nitride occurs through cyano group formation. The evolution of HCN already at 570-600 ºC was reported also in some cases.[43] The synthesis temperatures used in this study (550 and 600 ºC) and a long time of annealing (4 h) are sufficient for the thermal

degradation of a part of heptazine rings to cyano groups. This supposition is justified by the fact that they were not observed in the case of the sample synthesized at 500 ºC and that their quantity rises with increasing the calcination temperature.

The N 1s spectrum has a complex structure with a clear signal at 398.7 eV and there exists a consensus on attributing it to pyridinic nitrogen in the heptazine (or triazine) ring (N1) - Fig. 3c. A clear shoulder at higher energies can be fitted using three curves having maxima at 399.4, 400.3, and 401.3 eV. They originate from primary amine (N2), secondary amine (N3), and quaternary nitrogen (N4), respectively.

The percentage of respective forms of nitrogen (based on XPS spectra) has been presented in Table 2. The ratios of N1 : N2 : N3 : N4 for respective samples are as follows:

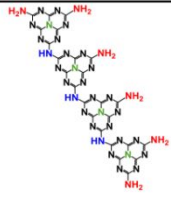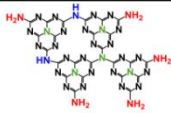|       | Py(N1) |   | NH$_2$(N2) |   | NH(N3) |   | Q(N4) |
|-------|--------|---|-----------|---|--------|---|-------|
| D-500 | 58     | : | 22        | : | 12     | : | 8     |
| D-550 | 62     | : | 17        | : | 11     | : | 9     |
| D-600 | 65     | : | 15        | : | 11     | : | 9     |

A clear rise in pyridinic nitrogen (N1) and a decrease in amino (N2) and imino (N3) nitrogen are observed with increasing temperature.

The obtained percentages of different forms of nitrogen should reflect atomic ratios in the real structure of carbon nitride. Can we reach such a conclusion and what are the contributions of respective forms of nitrogen to the structure of carbon nitride? The percentage of respective forms of nitrogen can be calculated by creating simple geometric models of carbon nitride consisting of heptazine subunits. In Table 3, models are presented of carbon nitrides based on the melon structure (the linear form of carbon nitride) and the fully condensed gCN (the network structure) as well as formulae with the use of which the number of atoms of a respective kind of nitrogen can be calculated. The melon structure can be regarded either as a single chain with increasing length (**Msc –** melon single-chain model) or as a model composed of many chains (**Mmc –** melon multi-chain model). It was assumed that in the network model (**Hn –** heptazine network), the number of heptazine subunits in X and Y directions is the same. The formulae presented in Table 3 enabled to calculate percentages of respective forms of nitrogen (N1, N2, N3, N4) in the different carbon nitride structures of increasing size (Table 3 and Fig. 4).

**Table 2** N 1s, C 1s and O 1s core level binding energies for graphitic carbon nitride condensed at different temperatures.

|       |       | 500 ºC | | | | 550 ºC | | | | 600 ºC | | | |
|-------|-------|---------|------|--------|-------|---------|------|--------|-------|---------|------|--------|-------|
|       |       | B.E., eV | FWHM | % Area | At.% | B.E., eV | FWHM | % Area | At.% | B.E., eV | FWHM | % Area | At.% |
| N 1s  | N1    | 398.7   | 1.17 | 57.5   | 23.44 | 398.7   | 1.0  | 62.5   | 31.30 | 398.7   | 1.0  | 64.8   | 32.67 |
|       | N2    | 399.6   | 1.17 | 22.2   | 9.04  | 399.5   | 1.0  | 17.1   | 8.55  | 399.4   | 1.0  | 15.2   | 7.64  |
|       | N3    | 400.5   | 1.17 | 12.1   | 4.93  | 400.4   | 1.0  | 11.3   | 5.68  | 400.3   | 1.0  | 11.1   | 5.58  |
|       | N4    | 401.4   | 1.17 | 8.2    | 3.34  | 401.4   | 1.0  | 9.1    | 4.57  | 401.3   | 1.0  | 9.0    | 4.56  |
|       |       | *Total N:* | | | *40.75* | *Total N:* | | | *50.09* | *Total N:* | | | *50.45* |
| C 1s  |       | 284.6   | 1.4  | 43.1   | 24.19 | 284.6   | 1.1  | 22.3   | 10.76 | 284.6   | 1.1  | 20.9   | 10.00 |
|       |       | -       | -    | -      | 0.00  | 287.0   | 1.1  | 0.8    | 0.38  | 286.9   | 1.0  | 1.4    | 0.69  |
|       |       | 288.0   | 1.2  | 56.9   | 31.96 | 288.2   | 1.1  | 76.9   | 37.19 | 288.2   | 1.0  | 77.7   | 37.2  |
|       |       | *Total C (in C-N):* | | | *31.96* | *Total C (in C-N):* | | | *37.57* | *Total C (in C-N):* | | | *37.89* |
| O 1s  |       | 533.1   | 2.7  | 100.0  | 3.10  | 532.8   | 2.5  | 100.0  | 1.58  | 532.6   | 2.5  | 100.0  | 1.67  |

**Table 3** Carbon nitride structures, equations for calculating the number of nitrogen atoms (N – number of heptazine subunits, n – number of chains) and the percentage of different forms of nitrogen.

| Carbon nitride structure | N | Nitrogen content, at.% | | | |
|---|---|---|---|---|---|
| | | Py (N1) | NH₂ (N2) | NH (N3) | Q (N4) |
| [structure] | 4-30 | 63.2-66.4 | 21.1-11.8 | 5.3-10.7 | 10.5-11.1 |
| Melon single-chain **Msc** | | $N*6$ | $N+2$ | $N-1$ | $N$ |
| [structure] | 2-30 | 64.3-65.5 | 17.9-14.5 | 7.1-9.1 | 10.7-10.9 |
| Melon multi-chain **Mmc** | | $N*6$ | $(N+2)*n$ | $(N-1)*n$ | $N*n$ |
| [structure] | 4-30 | 66.7-71.7 | 13.9-4.8 | 5.6-3.6 | 13.9-19.9 |
| Heptazine network **Hn** | | $N*6$ | $(\sqrt{N}*2)+1$ | $(\sqrt{N}-1)*2$ | $(\sqrt{N}-1)^2+N$ |

Percentages of nitrogen forms in the samples synthesized from dicyandiamide at 500, 550, and 600 $^{\circ}$C, as determined from the XPS studies, are presented in Fig. 4. Theoretical calculations[33-35] show that the most stable form of carbon nitride is the structure composed of tri-s-triazine (heptazine) units, therefore we may eliminate the triazine network model from our considerations. A frequently suggested carbon nitride structure is the fully condensed heptazine network (Hn). It results from the geometric model, which was assumed by us, that pyridinic nitrogen content (N1) should range from 66.7 to 71.7 % (beginning from the smallest to the greatest structures). The structures consisting of 10 subunits contain 70 % nitrogen N1. However, the percentage of nitrogen N1 in the studied samples is considerably lower and increases with rising temperature in order 57.5, 62.5, 64.8 % (Table 2). This discrepancy indicates that the Hn model not necessarily describes correctly the structure obtained by us. The quaternary nitrogen (N4) content also undermines it. In the Hn model, it should range between 13.9-19.9 % (Table 3), whereas in our samples it is lower, namely from 8.2 to 9.1 % (Table 2). Moreover, the theoretical content of amino nitrogen, according to the Hn model should be 13.9% for the structures consisting of 4 subunits and 4.8% for the structures composed of 30 heptazine subunits (Table 3). The XPS measurements show the values ranging from 15.2-22.2 % (Table 2), which are considerably higher than those predicted by the Hn model. This means that the measured contents of the respective forms of nitrogen are out of tune with the theoretical predictions for the model of fully condensed carbon nitride.

A better fitting of experimental data was observed by using models based on the chain structure of melon – melon single-chain (Msc) and melon multi-chain (Mmc). The later reflects the real composition of samples particularly well. The real content of nitrogen N1 perfectly fits into the Mmc model – the XPS
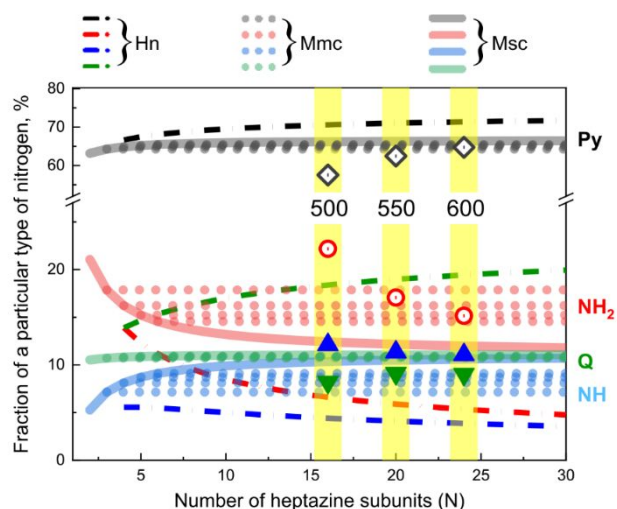


**Fig. 4** The content of different forms of nitrogen in various models of carbon nitride: Hn (heptazine network) – the model consisting of heptazine building blocks connected into a network, Mmc (melon multi-chain) – the model based on melon built of many chains, Msc (melon single-chain) – the model based on melon built of one chain. The results of XPS measurements of the composition of carbon nitride synthesized at 500, 550 and 600 $^{\circ}$C are also presented in the Figure. ◈ - Py nitrogen (N1), ⊙ - NH₂ nitrogen (N2), ▲ - NH nitrogen (N3), ▼ - quaternary nitrogen (N4).

results almost exactly lie on the theoretical curve (Fig. 4). A similar agreement occurs for amino nitrogen N2. The real contents of nitrogen N4 are somewhat lower than those predicted by the Mmc model (by about 1-2 %). In turn, there is somewhat more nitrogen N3 (−NH groups) than predicted by the theoretical model. The increased content of nitrogen N3 can be elucidated by the presence of nitrile species −C≡N which were observed in the C 1s spectrum and which give a signal at ~400.1 eV in the N 1s spectrum.[62] The small content of −C≡N groups in the samples and the proximity of the position to that of the peak from −NH (400.5 eV) caused that they are indistinguishable and reckoned to the −NH (N3) peak and this explains the observed higher content of nitrogen N3 in the samples. It worth to remind that nitrile groups can be formed at high temperatures by the decomposition of heptazine rings[61] which in turn, reduces the amount of quaternary nitrogen (N4). A comparison of the real content of respective forms of nitrogen in carbon nitride samples to theoretical predictions shows that only melon multi-chain correctly reflects the quantitative experimental data obtained from the XPS measurements. It should be assumed that the carbon nitride formed is a linear melon-type form rather than a fully condensed network structure (Hn). The above considerations bring to a general conclusion that the interpretation of XPS spectra should not be limited to its qualitative analysis. Quantitative analysis of respective nitrogen forms should always be conducted and only on this basis a final conclusion on carbon nitride structure can be drawn.

## 3.2. The determination of crystal structure by X-ray powder diffraction (XRD)

The crystal structure of 3D graphitic carbon nitride arouses many controversies. In the literature, two main models were reported. One of them is based on the structure of fully polymerized polyheptazine (Fig. 5a) and the other one, on partially polymerized, where heptazine subunits form poly(aminoimino)heptazine chains (called melon) (Fig. 5b). The structure of fully-condensed carbon nitride is described by the hexagonal cell [63, 64] and space group P6m2,[65] whereas the linear structure of melon-type by the orthorhombic cell and space group P2$_1$2$_1$2 proposed by Lotsch et al.[36] Fina et al.[66] and by Seyfarth et al.[67]

In Fig. 6 the X-ray diffraction pattern of carbon nitride prepared by us at 600 °C was juxtaposed with theoretical models calculated for unit cells P6m2 and P2$_1$2$_1$2 and intensities and positions of reflections determined theoretically for ideal unit cells of hexagonal P6m2 (187) and orthorhombic P2$_1$2$_1$2 (18) systems.

Many authors point at the hexagonal model because it results from the basic information provided by the powder diffraction pattern with an annular alternate arrangement of carbon and nitrogen atoms and the formation of layers connected by van der Waals interactions. It creates opportune conditions for the formation of more and more number of symmetry elements, which translates into a smaller number of reflections in the XRD spectrum. However, even a superficial analysis of Fig. 6 allows
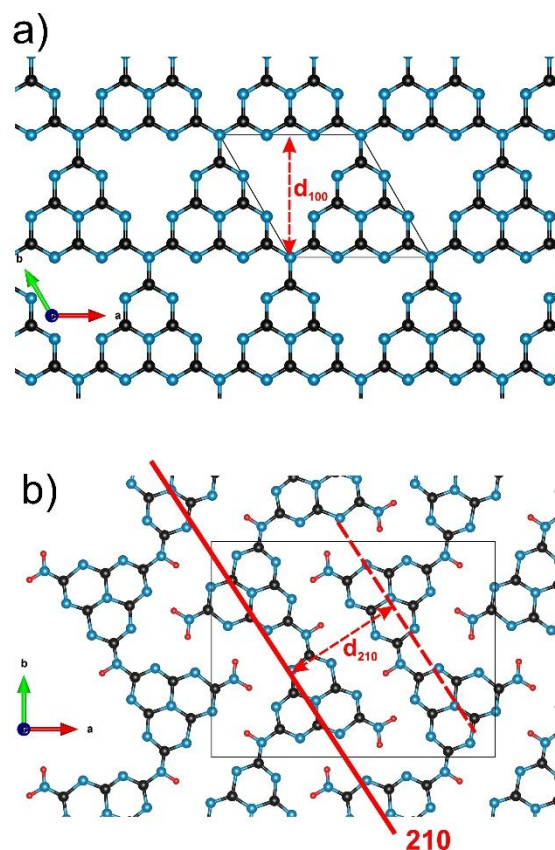


**Fig. 5** The structure of heptazine-based graphitic carbon nitride, a) polyheptazine (fully-condensed), and b) poly(aminoimino)heptazine (melon-type). Carbon, nitrogen and hydrogen atoms are represented as black, blue and red spheres, respectively.

to conclude that the orthorombic system for the melon-type graphitic carbon nitride (model A) better describes the structure of the studied material than the hexagonal system. In B model, peaks at 10.8, 17.7 21.9 2Θ are missing which explicitly indicates the occurrence of an order lower than hexagonal.
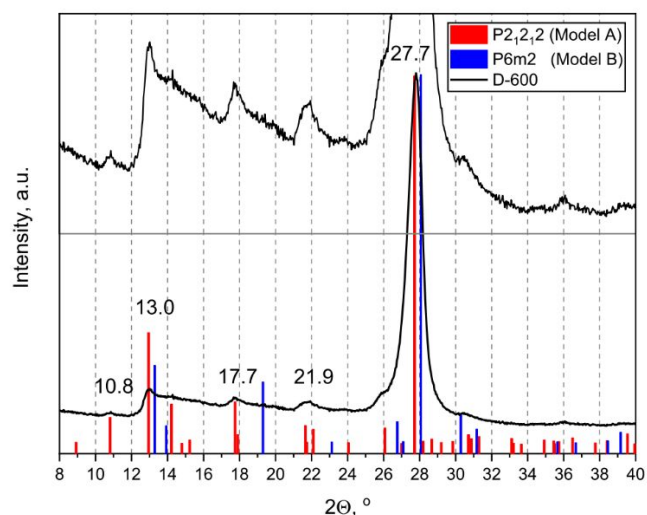


**Fig. 6** XRD patterns of D-600 carbon nitride obtained experimentally (black line) and theoretically calculated fully condensed hexagonal P6m2 cell (blue) and orthorhombic melon-type P21212 cell (red). The upper part of the figure is an enlargement of the bottom diffraction pattern.

**Journal Name** ARTICLE
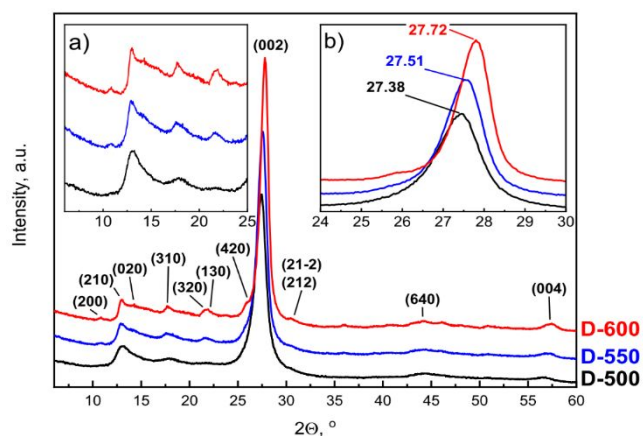


**Fig. 7** X-ray powder diffraction patterns of gCN–C₃N₄ synthesized at different temperatures; a) enlargement of the range 6-25° 2Θ; b) enlargement of the range 24-30° 2Θ.

The XRD patterns of gCN samples obtained at different temperatures are presented in Fig. 7. All gCN samples on the powder diffraction spectra contain several broad reflections that confirm their nanocrystalline (or even amorphous) nature. All the XRD patterns have a major strong peak at about 27.5° 2Θ, which is indicative of a layered component with an interlayer spacing of ~3.2 Å (Fig. 7). With a rise in the synthesis temperature, the peak at ~27.5° 2Θ becomes more and more intense and sharper. It shifts to greater 2Θ angles, which indicates an increase in the system order; the crystallites become larger and the interplanar spacing $d$ decreases from 3.254 Å do 3.215 Å (see Table 4). This indicates an increase in the number of layers parallel to the 002 plane as a result of the continuous condensation process of carbon nitride chains with increasing temperature until the system becomes stable (Table 4). A confirmation of this phenomenon is a small but noticeable increase in the size of crystallites in the direction of the c axis of the unit cell as determined using the Scherrer equation (Table 4).[68] The aforementioned rise in the size of crystallites in the direction of the c axis means that the number of condensed layers increases. Graphitic carbon nitride synthesized at 500 °C consists of 22 layers, whereas that synthesized at 600 °C has 31 layers. The above considerations about the size of crystallites and number of condensed layers should be regarded as approximate because there exists an additional factor influencing the relative reduction in the intensity of hk0 reflections in the powder diffraction pattern of the gCN structure, namely the translation of flat defects in the neighbouring layers which causes the displacement of layers. These displacements are responsible for the increase in the disorder of 3D structure in compliance with the model proposed by Seyfarth et al.[67] and Lotsch et al.[36] The low angle signal at about 13° 2Θ corresponds to the distance $d$ = 6.8 Å and can be indexed as the reflection (210) which refers to the distance between two adjacent melon chains in the crystal (Fig. 5b).[36, 47, 66, 69] Also in this case, a gradual decrease in the d-spacing with increasing condensation temperature (from 6.857 to 6.797 Å – see Table 4) is observed.

**Table 4** Unit cell and structural parameters of gCN synthesized at different temperatures (space group P2₁2₁2, No. 18). The measurement error is given in parentheses. The structure models used for the refinement of gCN were placed in the ESI.

| Temperature [°C] | 500 | 550 | 600 |
|---|---|---|---|
| (002) [2Θ] | 27.380 | 27.508 | 27.723 |
| (002) d [Å] | 3.254 | 3.234 | 3.215 |
| a [Å] | 16.352(6) | 16.264(6) | 16.351(6) |
| b [Å] | 12.497(4) | 12.386(4) | 12.309(4) |
| c [Å] | 6.5018(4) | 6.4682(5) | 6.4379(4) |
| V [Å³] | 1328.67(58) | 1303.01(56) | 1307.92(26) |
| size₍₀ ₀ ₂₎ [nm] | 7 | 8 | 10 |
| number of layers | 22 | 25 | 31 |
| (210) [2Θ] | 12.900 | 12.945 | 13.014 |
| (210) d [Å] | 6.857 | 6.833 | 6.797 |

As shown above, X-ray diffraction patterns of carbon nitride samples obtained by the thermal condensation of dicyandiamide can be described correctly only by assuming the orthorombic system with the space group P2₁2₁2 and presuming that the layers are formed from the chains of poly(aminoimino)heptazine (melon). The results are consistent with those drawn from the XPS study.

## 3.3. Summary

The paper presents results of structural studies of graphitic carbon nitrides obtained by the thermal condensation of dicyandiamide in a semi-closed system with the access of air. This method is the most frequently used, the simplest and the cheapest for the synthesis of graphitic carbon nitride.

It results from this study that carbon nitride prepared by the thermal condensation consists of melon chains as suggested earlier by Miller et al. [30] and Kessler et al.,[32] rather than fully condensed polyheptazine structure. This is testified by the relative ratios of pyridinic, amino, imino, and quaternary nitrogen obtained from XPS analysis. These ratios correspond to the melon structure and are out of tune with the fully condensed structure. Such a conclusion is also confirmed by the XRD results which proved that the 3D crystal structure of carbon nitride can be correctly described only by the orthorombic cell and space group P2₁2₁2 applied to condensed chains of poly(aminoimino)heptazine (melon). Both XPS and XRD studies have shown that a rise in the synthesis temperature results in the increase in the condensation degree and the degree of structural order of carbon nitride. The interplanar distance $d$ decreases systematically with the rise in the synthesis temperature and at the same time the number of condensed layers increases. Moreover, it was shown that the XPS investigation should not be limited to qualitative studies. Only quantitative XPS analysis allows us to correctly identify the carbon nitride structure.

## Conflicts of interest

There are no conflicts to declare.

## Acknowledgements

## References

1. X. C. Wang, K. Maeda, A. Thomas, K. Takanabe, G. Xin, J. M. Carlsson, K. Domen and M. Antonietti, *Nat. Mater.*, 2009, **8**, 76-80.
2. J. Liu, Y. Liu, N. Y. Liu, Y. Z. Han, X. Zhang, H. Huang, Y. Lifshitz, S. T. Lee, J. Zhong and Z. H. Kang, *Science*, 2015, **347**, 970-974.
3. S. C. Yan, Z. S. Li and Z. G. Zou, *Langmuir*, 2009, **25**, 10397-10401.
4. S. W. Cao, J. X. Low, J. G. Yu and M. Jaroniec, *Adv. Mater.*, 2015, **27**, 2150-2176.
5. G. Liu, P. Niu, C. H. Sun, S. C. Smith, Z. G. Chen, G. Q. Lu and H. M. Cheng, *J. Am. Chem. Soc.*, 2010, **132**, 11642-11648.
6. Y. J. Zhang, T. Mori, J. H. Ye and M. Antonietti, *J. Am. Chem. Soc.*, 2010, **132**, 6294-6295.
7. Z. Z. Lin and X. C. Wang, *Angew. Chem. Int. Ed.*, 2013, **52**, 1735-1738.
8. L. B. Jiang, X. Z. Yuan, Y. Pan, J. Liang, G. M. Zeng, Z. B. Wu and H. Wang, *Appl. Catal. B*, 2017, **217**, 388-406.
9. M. Q. Xu, B. Chai, J. T. Yan, H. B. Wang, Z. D. Ren and K. W. Paik, *NANO*, 2016, **11**, 11.
10. Z. K. Zhao, Y. T. Dai, J. H. Lin and G. R. Wang, *Chem. Mater.*, 2014, **26**, 3151-3161.
11. Y. P. Zhu, T. Z. Ren and Z. Y. Yuana, *ACS Appl. Mater. Interfaces*, 2015, **7**, 16850-16856.
12. P. F. Zhang, H. Y. Zhu and S. Dai, *ChemCatChem*, 2015, **7**, 2788-2805.
13. X. B. Li, A. F. Masters and T. Maschmeyer, *ChemCatChem*, 2015, **7**, 121-126.
14. Q. Han, B. Wang, Y. Zhao, C. G. Hu and L. T. Qu, *Angew. Chem. Int. Ed.*, 2015, **54**, 11433-11437.
15. H. Xu, Z. Wu, Y. T. Wang and C. S. Lin, *J. Mater. Sci.*, 2017, **52**, 9477-9490.
16. Y. Z. Cao, Q. Li and W. Wang, *RSC Adv.*, 2017, **7**, 6131-6139.
17. Z. W. Zhao, Y. J. Sun and F. Dong, *Nanoscale*, 2015, **7**, 15-37.
18. X. C. Gao, J. Feng, D. W. Su, Y. C. Ma, G. X. Wang, H. Y. Ma and J. T. Zhang, *Nano Energy*, 2019, **59**, 598-609.
19. I. Papailias, N. Todorova, T. Giannakopoulou, N. Ioannidis, N. Boukos, C. P. Athanasekou, D. Dimotikali and C. Trapalis, *Appl. Catal. B*, 2018, **239**, 16-26.
20. J. Feng, T. T. Chen, S. N. Liu, Q. H. Zhou, Y. M. Ren, Y. Z. Lv and Z. J. Fan, *J. Colloid Interface Sci.*, 2016, **479**, 1-6.
21. J. C. Tong, L. Zhang, F. Li, K. Wang, L. F. Han and S. K. Cao, *RSC Adv.*, 2015, **5**, 88149-88153.
22. F. Dong, Y. H. Li, Z. Y. Wang and W. K. Ho, *Appl. Surf. Sci.*, 2015, **358**, 393-403.
23. Y. Zheng, Z. S. Zhang and C. H. Li, *J. Photochem. Photobiol. A-Chem.*, 2017, **332**, 32-44.
24. W. D. Zhang, Q. Zhang, F. Dong and Z. W. Zhao, *Int. J. Photoenergy*, 2013, DOI: 10.1155/2013/685038, 9.
25. S. Martha, A. Nashim and K. M. Parida, *J. Mater. Chem. A*, 2013, **1**, 7816-7824.
26. Y. W. Zhang, J. H. Liu, G. Wu and W. Chen, *Nanoscale*, 2012, **4**, 5300-5303.
27. G. G. Zhang, J. S. Zhang, M. W. Zhang and X. C. Wang, *J. Mater. Chem.*, 2012, **22**, 8083-8091.
28. A. Thomas, A. Fischer, F. Goettmann, M. Antonietti, J. O. Muller, R. Schlogl and J. M. Carlsson, *J. Mater. Chem.*, 2008, **18**, 4893-4908.
29. B. Jurgens, E. Irran, J. Senker, P. Kroll, H. Muller and W. Schnick, *J. Am. Chem. Soc.*, 2003, **125**, 10288-10300.
30. T. S. Miller, A. B. Jorge, T. M. Suter, A. Sella, F. Cora and P. F. McMillan, *Phys. Chem. Chem. Phys.*, 2017, **19**, 15613-15638.
31. T. S. Miller, A. d'Aleo, T. Suter, A. E. Aliev, A. Sella and P. F. McMillan, *Z. Anorg. Allg. Chem.*, 2017, **643**, 1572-1580.
32. F. K. Kessler, Y. Zheng, D. Schwarz, C. Merschjann, W. Schnick, X. C. Wang and M. J. Bojdys, *Nat. Rev. Mater.*, 2017, **2**, 17.
33. J. Sehnert, K. Baerwinkel and J. Senker, *J. Phys. Chem. B*, 2007, **111**, 10671-10680.
34. E. Kroke, M. Schwarz, E. Horath-Bordon, P. Kroll, B. Noll and A. D. Norman, *New J. Chem.*, 2002, **26**, 508-512.
35. J. Gracia and P. Kroll, *J. Mater. Chem.*, 2009, **19**, 3013-3019.
36. B. V. Lotsch, M. Doblinger, J. Sehnert, L. Seyfarth, J. Senker, O. Oeckler and W. Schnick, *Chem. Eur. J.*, 2007, **13**, 4969-4980.
37. G. Greczynski and L. Hultman, *Prog. Mater Sci.*, 2020, **107**, 46.
38. T. J. B. Holland and S. A. T. Redfern, *Mineral. Mag.*, 1997, **61**, 65-77.
39. T. Roisnel and J. Rodríquez-Carvajal, *Mater. Sci. Forum*, 2001, **378-381**, 118-123.
40. E. Broitman, J. Neidhardt and L. Hultman, in *Tribology of Diamond-Like Carbon Films: Fundamentals and Applications*, Springer US, 2008, DOI: 10.1007/978-0-387-49891-1_24, pp. 620-653.
41. L. N. Zhang, H. Wang, W. Z. Shen, Z. F. Qin, J. G. Wang and W. B. Fan, *J. Catal.*, 2016, **344**, 293-302.
42. J. Xu, T. Chen, Q. Jiang and Y. X. Li, *Chemistry-an Asian Journal*, 2014, **9**, 3269-3277.
43. V. W. H. Lau, M. B. Mesch, V. Duppel, V. Blum, J. Senker and B. V. Lotsch, *J. Am. Chem. Soc.*, 2015, **137**, 1064-1072.
44. H. Z. Dai, X. C. Gao, E. Z. Liu, Y. H. Yang, W. Q. Hou, L. M. Kang, J. Fan and X. Y. Hu, *Diamond Relat. Mater.*, 2013, **38**, 109-117.
45. Z. P. Chen, E. Vorobyeva, S. Mitchell, E. Fako, N. Lopez, S. M. Collins, R. K. Leary, P. A. Midgley, R. Hauert and J. Perez-Ramirez, *Natl. Sci. Rev.*, 2018, **5**, 642-652.
46. K. D. Bartle, D. L. Perry and S. Wallace, *Fuel Process. Technol.*, 1987, **15**, 351-361.
47. K. Akaike, K. Aoyama, S. Dekubo, A. Onishi and K. Kanai, *Chem. Mater.*, 2018, **30**, 2341-2352.
48. K. Stańczyk, R. Dziembaj, Z. Piwowarska and S. Witkowski, *Carbon*, 1995, **33**, 1383-1392.
49. M. A. Wójtowicz, J. R. Pels and J. A. Moulijn, *Fuel*, 1995, **74**, 507-516.
50. D. M. Feng, Z. M. Zhou and M. P. Bo, *Polym. Degrad. Stab.*, 1995, **50**, 65-70.

Dalton Transactions

51. H. Schmiers, J. Friebel, P. Streubel, R. Hesse and R. Kopsel, *Carbon*, 1999, **37**, 1965-1978.
52. S. R. Kelemen, M. Afeworki, M. L. Gorbaty, P. J. Kwiatek, M. S. Solum, J. Z. Hu and R. J. Pugmire, *Energy Fuels*, 2002, **16**, 1507-1515.
53. C. Z. Zhang, R. Hao, H. B. Liao and Y. L. Hou, *Nano Energy*, 2013, **2**, 88-97.
54. Y. O. Wang, M. K. Bayazit, S. J. A. Moniz, Q. S. Ruan, C. C. Lau, N. Martsinovich and J. W. Tang, *Energy Environ. Sci.*, 2017, **10**, 1643-1651.
55. J. Cai, Y. Han, S. Y. Chen, E. J. Crumlin, B. Yang, Y. M. Li and Z. Liu, *J. Phys. Chem. C*, 2019, **123**, 12176-12182.
56. F. Tao, Z. H. Wang, M. H. Qiao, Q. Liu, W. S. Sim and G. Q. Xu, *J. Chem. Phys.*, 2001, **115**, 8563-8569.
57. P. Brant, J. H. Enemark and A. L. Balch, *J. Organomet. Chem.*, 1976, **114**, 99-106.
58. S. Lalitha and P. T. Manoharan, *J. Electron Spectrosc. Relat. Phenom.*, 1989, **49**, 61-75.
59. C. R. Wu, W. R. Salaneck, J. J. Ritsko and J. L. Bredas, *Synth. Met.*, 1986, **16**, 147-159.
60. G. P. Wu, C. X. Lu, X. P. Wu, S. C. Zhang, H. Fu and L. C. Ling, *J. Appl. Polym. Sci.*, 2004, **94**, 1705-1709.
61. R. C. Dante, P. Martin-Ramos, A. Correa-Guimaraes and J. Martin-Gil, *Mater. Chem. Phys.*, 2011, **130**, 1094-1102.
62. H. J. Yu, R. Shi, Y. X. Zhao, T. Bian, Y. F. Zhao, C. Zhou, G. I. N. Waterhouse, L. Z. Wu, C. H. Tung and T. R. Zhang, *Adv. Mater.*, 2017, **29**, 8.
63. L. H. Amorin, V. Y. Suzuki, N. H. de Paula, J. L. Duarte, M. A. T. da Silva, C. A. Taft and F. D. La Porta, *New J. Chem.*, 2019, **43**, 13647-13653.
64. G. Xu, Y. H. Xu, Z. C. Zhou and Y. W. Bai, *Diamond Relat. Mater.*, 2019, **97**, 9.
65. T. Tyborski, C. Merschjann, S. Orthmann, F. Yang, M. C. Lux-Steiner and T. Schedel-Niedrig, *J. Phys. Condens. Matter.*, 2013, **25**, 7.
66. F. Fina, S. K. Callear, G. M. Carins and J. T. S. Irvine, *Chem. Mater.*, 2015, **27**, 2612-2618.
67. L. Seyfarth, J. Seyfarth, B. V. Lotsch, W. Schnick and J. Senker, *Phys. Chem. Chem. Phys.*, 2010, **12**, 2227-2237.
68. A. S. Vorokh, *Nanosyst.-Phys. Chem. Math.*, 2018, **9**, 364-369.
69. J. Q. Wen, J. Xie, X. B. Chen and X. Li, *Appl. Surf. Sci.*, 2017, **391**, 72-123.